Electric Power Systems Research 203 (2022) 107627

Contents lists available at ScienceDirect

Electric Power Systems Research

journal homepage: www.elsevier.com/locate/epsr

# Numerical analysis and safety design of grounding systems in underground compact substations

R. Guizán [a], I. Colominas [*,a], J. París [a], I. Couceiro [a], F. Navarrina [a]

*Universidade da Coruña, Group of Numerical Methods in Engineering-GMNI, Center for Technological Innovation in Construction and Civil Engineering-CITEEC. Civil Engineering School, Campus de Elviña, A Coruña 15071, Spain*

ARTICLE INFO

*Keywords:*
Grounding systems
Potential distributions
Underground substations

ABSTRACT

This paper presents a mathematical and numerical formulation to design and analyze grounding systems in underground electrical substations. The developed approach is based on the well known Maxwell's Equations. The proposed problem is solved by means of the Boundary Element Method (BEM). The utilization of BEM allows to introduce the geometry and electrical characteristics of the enclosure in a uniform soil. Therefore, a more realistic approximation of the soil structure is achieved. This formulation allows to obtain the main parameters of these protection systems (the grid resistance, the Ground Potential Rise, and the step and mesh voltage). It also allows to compute the surface and step voltage distributions. In addition, as a secondary result, the voltage and current density distributions over the enclosure are obtained. Finally, two grounding system analyses of real underground electrical substations are presented to demonstrate the industrial application and the modelization capabilities of the proposed formulation.

## 1. Introduction

It is widely known that most electricity consumers live and work at cities and urban areas which have experienced significant growth in the last decades. Consequently, the demand for power supply has increased and the electricity supply should always be ensured, building and installing new electrical substations in urban areas is required. However, this construction is not so simple due to some drawbacks as the urban environmental restrictions or the limited availability of space. Against this background, engineers developed the underground electrical substations.

Underground electrical substations are compact solutions where all the electrical equipment is placed underground inside precast concrete enclosures. One of its main characteristics is that the area occupied aboveground is minimum and therefore they meet the urban environmental requirements and they are suitable for zones with limited space for their location. A critical aspect in this substations, as in other electrical facilities, is safety, especially during a fault situation in order to prevent electric shocks [1]. In electrical substations, the grounding systems are the devices in charge of guaranteeing the safety conditions and the functioning of these facilities. Therefore, their design and analysis are essential.

Since the beginning of aboveground electrical substations, numerous researches were developed to analyze their grounding systems [2]. In this context, analytical [3,4], semianalytical [5] or numerical methods [6,7] had been carried out and applied to uniform, two-layer or multilayer soil models. Recently, more advanced studies analyze the phenomenon of transferred potentials [8] or the presence of soil heterogeneities [9]. However, these researches are never applied to underground electrical substations.

In previous works, the authors have developed a general formulation based on BEM to design and analyze the grounding system of aboveground electrical substations considering uniform [10] and layered soil models [11,12]. In 2015, the authors started the grounding system analysis in underground electrical substations [13].

This paper presents a mathematical and numerical approach to analyze and calculate properly the main parameters of grounding systems of underground electrical substations. The developed formulation allows to introduce the geometrical and electrical properties of the precast concrete enclosure in a uniform soil and, therefore, more realistic results are obtained in comparison with the standard formulations. The formulation could be expanded in order to deal with multilayer soil models. The methodology generated has been validated against benchmark examples from the IEEE [14]. A deeper detail of the formulation

* Corresponding author.
*E-mail address:* icolominas@udc.es (I. Colominas).

https://doi.org/10.1016/j.epsr.2021.107627
Received 2 June 2021; Received in revised form 22 September 2021; Accepted 11 October 2021
Available online 23 October 2021

developed and its validation can be found in [15].

## 2. Mathematical and numerical model

### 2.1. Equations of the mathematical model

During a fault situation in an electrical substation, the fault current originated is derived from the electrical facility to the grounding system, which will be dissipated into the ground causing potential gradients in the surrounding area.

The formulation developed to analyze this physical phenomenon is based on the Maxwell's Equations, which define the behavior of an electric current flow in a 3D domain. The transient period is extremely short in comparison with the fault duration, so the study of fault current discharges will be limited to the steady-state behavior [14]. Therefore, the general equations that define the physical phenomenon described in a generic conductive medium ($\Omega$) and at the interface of different media ($\partial\Omega$) are:

1. Coulomb's equations:

$$\begin{aligned} \mathbf{div}(\mathbf{E}) &= \frac{q_v}{\epsilon_0} \quad \text{in} \quad \Omega \\ \mathbf{rot}(\mathbf{E}) &= \mathbf{0} \quad \text{in} \quad \Omega \\ \mathbf{n}\cdot(\mathbf{E}_2 - \mathbf{E}_1) &= \frac{q_s}{\epsilon_0} \quad \text{in} \quad \partial\Omega \\ \mathbf{n}\times(\mathbf{E}_2 - \mathbf{E}_1) &= \mathbf{0} \quad \text{in} \quad \partial\Omega \end{aligned} \tag{1}$$

where $\mathbf{E}$ is the electric field, $q_v$ is the electric charge density, $q_s$ is the surface electric charge density, $\epsilon_0$ is the vacuum permittivity ($8.8542 \times 10^{-12}$ F/m), and $\mathbf{n}$ is the unit vector normal to the boundary $\partial\Omega$.

1. The continuity equation:

$$\begin{aligned} \mathbf{div}(\boldsymbol{\sigma}) &= 0 \quad \text{in} \quad \Omega \\ \mathbf{n}\cdot(\boldsymbol{\sigma}_2 - \boldsymbol{\sigma}_1) &= 0 \quad \text{in} \quad \partial\Omega \end{aligned} \tag{2}$$

where $\boldsymbol{\sigma}$ is the electric current density.

1. The constitutive equation:

$$\boldsymbol{\sigma} = \boldsymbol{\gamma}\,\boldsymbol{E} \quad \text{in} \quad \Omega \tag{3}$$

where $\boldsymbol{\gamma}$ is the conductivity tensor.

In order to obtain the mathematical model, each of these equations will be applied to each domain and boundary of the problem (Fig. 1). It should be noted that in this problem the hypotheses that the atmosphere ($\Omega_A$) is a perfect insulator and the grounding grid ($\Omega_G$) is formed by perfect conductors are assumed. Furthermore, the soil structure is composed of a uniform soil, the ground ($\Omega$), which has a non-homogenous finite volume inside, the underground electrical substation ($\Omega_I$). The procedure followed consists on studying independently each conductive subregion ($\Omega$ and $\Omega_I$), and then, the obtained equations

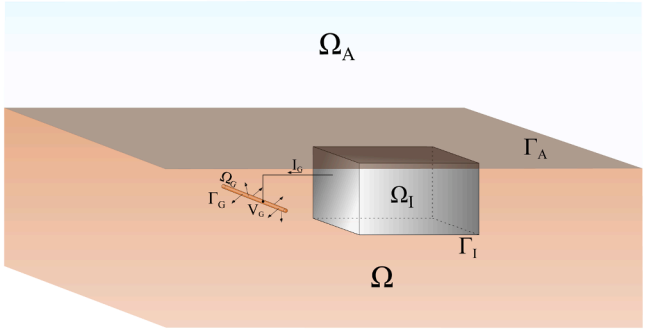


**Fig. 1.** Domains involved in the problema analyzed.

are coupled to solve them by means of the compatibility condition. An in-depth analysis of this procedure can be found in [15].

Since the ground surface is considered horizontal, the mathematical problem is transformed to an easier one by means of the application of the method of images [11]. As a result, the physical phenomenon of a fault situation in an underground electrical substation is mathematically defined as:

1. An exterior Dirichlet problem in $\Omega$ with boundary conditions in $\Gamma_G$ and $\Gamma_G^{'}$:

$$\begin{aligned} \Delta V &= 0 \quad \text{in} \quad \Omega \\ V &= V_G \quad \text{in} \quad \Gamma_G \quad \text{and} \quad \Gamma_G^{'} \\ V &\text{satisfies regularity conditions at infinity} \end{aligned} \tag{4}$$

where $V$ is the potential in the ground and satisfies regularity conditions at infinity, $V_G$ is the ground potential rise (GPR), and $\Gamma_G$ and $\Gamma_G^{'}$ are the grounding grid surfaces.

1. Two interior problems in $\Omega_I$ and $\Omega_I^{'}$:

$$\Delta V_I = 0 \quad \text{in} \quad \Omega_I \quad \text{and} \quad \Omega_I^{'} \tag{5}$$

where $V_I$ is the potential on the enclosure surface.

1. And the boundary conditions in $\Gamma_I$ and $\Gamma_I^{'}$, which are the compatibility condition between the exterior and the interior problems:

$$\begin{aligned} V_I &= V \quad \text{in} \quad \Gamma_I \quad \text{and} \quad \Gamma_I^{'} \\ \mathbf{n}\cdot\boldsymbol{\sigma}_I &= \mathbf{n}\cdot\boldsymbol{\sigma} \quad \text{in} \quad \Gamma_I \quad \text{and} \quad \Gamma_I^{'} \end{aligned} \tag{6}$$

where $\boldsymbol{\sigma}$ and $\boldsymbol{\sigma}_I$ are the current densities in the ground and the enclosure, respectively, and $\Gamma_I$ and $\Gamma_I^{'}$ are the enclosure surfaces.

The resolution of these equations will allow to calculate the main parameters of a grounding grid, which are principally the ground resistance, the step and touch voltages, and the earth surface potential. Then, the safety conditions during a fault situation can be analyzed.

### 2.2. Boundary integral equations (BIEs)

The first step to solve the previous equations consists on transforming the differential problems defined into integral equations relating only boundary values. The obtention of these BIEs will provide the starting point to solve the potential problems by the BEM and make the mathematical model more practical for the subsequent numerical analysis. This transformation starts from the expression that mathematically defined the Green's second identity:

$$\int\int\int_V (\varphi\Delta\psi - \psi\Delta\varphi)dV = \int\int_S (\varphi\nabla\psi\cdot\boldsymbol{n} - \psi\nabla\varphi\cdot\boldsymbol{n})dS \tag{7}$$

where the function $\varphi$ will be substituted for the potential field $V$ (exterior Dirichlet problem) or $V_I$ (interior problem), and the function $\psi$ will be the fundamental solution of the Laplace equation for a three-dimensional potential problem:

$$\psi(\boldsymbol{x},\boldsymbol{y}) = \frac{1}{4\pi r(\boldsymbol{x},\boldsymbol{y})} \tag{8}$$

where $r(\boldsymbol{x},\boldsymbol{y})$ is the distance between the source point $\boldsymbol{x}$ and the field point $\boldsymbol{y}$.

Then, problems (4) and (5) are recast independently into integral equations by means of expression (7), as well as the compatibility condition (6).

As a result, the differential equations of the mathematical model are

formulated as the following three BIEs:

1. Equation from the boundary condition of the exterior Dirichlet problem $V(\chi_G) = V_G$:

$$\begin{aligned}
&\frac{1}{4\pi\gamma}\int\int_{\xi_G\in\Gamma_G}\left(\frac{1}{r(\chi_G,\xi_G)}+\frac{1}{r(\chi_G^{'},\xi_G)}\right)\sigma_G(\xi_G)\,\mathrm{d}\Gamma_G+\\
&\frac{1}{4\pi\gamma}\int\int_{\xi_I\in\Gamma_I}\left(\frac{1}{r(\chi_G,\xi_I)}+\frac{1}{r(\chi_G^{'},\xi_I)}\right)\sigma_I(\xi_I)\,\mathrm{d}\Gamma_I+\\
&\frac{1}{4\pi}\int\int_{\xi_I\in\Gamma_I}\left[\left(\nabla\left(\frac{1}{r(\chi_G,\xi_I)}\right)+\nabla\left(\frac{1}{r(\chi_G^{'},\xi_I)}\right)\right)\cdot\mathbf{n}(\xi_I)\right]\\
&V_I(\xi_I)\,\mathrm{d}\Gamma_I = V_G
\end{aligned}\tag{9}$$

where $\chi_G$ and $\chi_G^{'}$ are source points located on surface $\Gamma_G$ and $\Gamma_G^{'}$, $\xi_G$ is a field point located on surface $\Gamma_G$, $\xi_I$ is a field point located on surface $\Gamma_I$, $\sigma_G(\xi_G)$ is the leakage current density on surface $\Gamma_G$, $\sigma_I(\xi_I)$ is the leakage current density on surface $\Gamma_I$, and $V_I(\xi_I)$ is the value of potential belonging to any point located on surface $\Gamma_I$.

1. Equation from the compatibility condition applied on the exterior Dirichlet problem:

$$\begin{aligned}
&\frac{1}{4\pi\gamma}\int\int_{\xi_G\in\Gamma_G}\left(\frac{1}{r(\chi_I,\xi_G)}+\frac{1}{r(\chi_I^{'},\xi_G)}\right)\sigma_G(\xi_G)\,\mathrm{d}\Gamma_G+\\
&\frac{1}{4\pi\gamma}\int\int_{\xi_I\in\Gamma_I}\left(\frac{1}{r(\chi_I,\xi_I)}+\frac{1}{r(\chi_I^{'},\xi_I)}\right)\sigma_I(\xi_I)\,\mathrm{d}\Gamma_I+\\
&\frac{1}{4\pi}\int\int_{\xi_I\in\Gamma_I}\left[\left(\nabla\left(\frac{1}{r(\chi_I,\xi_I)}\right)+\nabla\left(\frac{1}{r(\chi_I^{'},\xi_I)}\right)\right)\cdot\mathbf{n}(\xi_I)\right]\\
&V_I(\xi_I)\,\mathrm{d}\Gamma_I = \frac{1}{2}V_I(\chi_I)
\end{aligned}\tag{10}$$

where $\chi_I$ and $\chi_I^{'}$ are source points located on surface $\Gamma_I$ and $\Gamma_I^{'}$.

1. Equation from the compatibility condition applied on the interior problem:

$$\begin{aligned}
\frac{1}{2}V_I(\chi_I) = -\ &\frac{1}{4\pi\gamma_I}\int\int_{\xi_I\in\Gamma_I}\frac{1}{r(\chi_I,\xi_I)}\,\sigma_I(\xi_I)\,\mathrm{d}\Gamma_I-\\
&\frac{1}{4\pi}\int\int_{\xi_I\in\Gamma_I}\left[\nabla\left(\frac{1}{r(\chi_I,\xi_I)}\right)\cdot\mathbf{n}(\xi_I)\right]V_I(\xi_I)\,\mathrm{d}\Gamma_I
\end{aligned}\tag{11}$$

These BIEs enable to calculate $\sigma_G$, $\sigma_I$, and $V_I$, which are the basic magnitudes in order to determine the main parameters of a grounding system.

One of these main parameters and an important point in grounding system analysis is the surface voltage distribution, which can be calculated by means of the following equation:

$$\begin{aligned}
V(\boldsymbol{x}) = \ &\frac{1}{4\pi\gamma}\int\int_{\xi_G\in\Gamma_G}\left(\frac{1}{r(\boldsymbol{x},\xi_G)}+\frac{1}{r(\boldsymbol{x}^{'},\xi_G)}\right)\sigma_G(\xi_G)\,\mathrm{d}\Gamma_G+\\
&\frac{1}{4\pi\gamma}\int\int_{\xi_I\in\Gamma_I}\left(\frac{1}{r(\boldsymbol{x},\xi_I)}+\frac{1}{r(\boldsymbol{x}^{'},\xi_I)}\right)\sigma_I(\xi_I)\,\mathrm{d}\Gamma_I+\\
&\frac{1}{4\pi}\int\int_{\xi_I\in\Gamma_I}\left[\left(\nabla\left(\frac{1}{r(\boldsymbol{x},\xi_I)}\right)+\nabla\left(\frac{1}{r(\boldsymbol{x}^{'},\xi_I)}\right)\right)\cdot\mathbf{n}(\xi_I)\right]\\
&V_I(\xi_I)\,\mathrm{d}\Gamma_I
\end{aligned}\tag{12}$$

where $V(\boldsymbol{x})$ is the value of the potential function in a source point $\boldsymbol{x}$ located in the ground.

The above equation can be simplified using the BIE obtained from the interior problem (11) as:

$$\begin{aligned}
V(\boldsymbol{x}) = &\frac{1}{4\pi\gamma}\int\int_{\xi_G\in\Gamma_G}\left(\frac{1}{r(\boldsymbol{x},\xi_G)}+\frac{1}{r(\boldsymbol{x}^{'},\xi_G)}\right)\sigma_G(\xi_G)\,\mathrm{d}\Gamma_G+\\
&\frac{1}{4\pi\gamma}\left(1-\frac{\gamma}{\gamma_I}\right)\int\int_{\xi_I\in\Gamma_I}\left(\frac{1}{r(\boldsymbol{x},\xi_I)}+\frac{1}{r(\boldsymbol{x}^{'},\xi_I)}\right)\sigma_I(\xi_I)\,\mathrm{d}\Gamma_I
\end{aligned}\tag{13}$$

This is the general equation to calculate the electric potential at any point in a uniform medium with a finite heterogeneity inside it.

Finally, these BIEs are solved numerically.

### 2.3. Numerical model

The adequate numerical method to solve this problem, where the equations are set in the boundaries of the domains, is the BEM.

The first step to address the numerical model is recast the BIEs (9)–(11) into their weak form. So that, this arrangement allows to obtain an accurate approximate solution of the problem through a weighted residual method. The weighted residual method chosen to develop the numerical approach of this problem is the point collocation [16], where the weighting function is the Dirac delta function.

In addition, in order to simplify the integral equations, an assumption of circumferential uniformity in the electrodes is made. This involves that the leakage current on the electrodes is supposed constant around the perimeter of every cross section ($\widehat{\sigma}_G$). This assumption is adequate and not too restrictive, taking into account that the electrodes used to be longer in comparison with their diameter. This procedure will allow to decouple the boundary integrals $\Gamma_G$ in integrals in the axial line of the electrodes $L_G$ and integrals in the circumferential perimeter $C_G$.

Thus, after formulating the BIEs into their weak forms, introducing the assumption of circumferential uniformity and applying the Point Collocation Method (PCM), the integral Eqs. (9)–(11) take the form:

1. Equation from the boundary condition of the exterior Dirichlet problem $V(\boldsymbol{\chi}_G) = V_G$

$$\begin{aligned}
&\pi\varphi\left(\widehat{\boldsymbol{\chi}}_{Gj}\right)V_G-\frac{1}{4\pi\gamma}\int_{\widehat{\xi}_G\in L_G}K\left(\widehat{\boldsymbol{\chi}}_{Gj},\widehat{\xi}_G\right)\,\widehat{\sigma}_G\left(\widehat{\xi}_G\right)\mathrm{d}L_G-\\
&\frac{1}{4\pi\gamma}\int\int_{\xi_I\in\Gamma_I}K\left(\widehat{\boldsymbol{\chi}}_{Gj},\boldsymbol{\xi}_I\right)\,\sigma_I(\xi_I)\,\mathrm{d}\Gamma_I-\\
&\frac{1}{4\pi}\int\int_{\xi_I\in\Gamma_I}K^{*}\left(\widehat{\boldsymbol{\chi}}_{Gj},\boldsymbol{\xi}_I\right)\,V_I(\xi_I)\,\mathrm{d}\Gamma_I=0\quad j=1,\ldots,n_{cp_G}
\end{aligned}\tag{14}$$

where $\varphi(\widehat{\boldsymbol{\chi}}_{Gj})$ is the diameter of electrodes, and $n_{cp_G}$ is the number of collocation points in $\Gamma_G$. Kernels $K(\widehat{\boldsymbol{\chi}}_{Gj},\widehat{\xi}_G)$, $K(\widehat{\boldsymbol{\chi}}_{Gj},\boldsymbol{\xi}_I)$ and $K^{*}(\widehat{\boldsymbol{\chi}}_{Gj},\boldsymbol{\xi}_I)$ are obtained after solving the integrals in the circumferential perimeter $C_G$.

1. Equation from the compatibility condition applied on the exterior Dirichlet problem:

$$\begin{aligned}
&\frac{1}{4\pi\gamma}\int_{\widehat{\xi}_G\in L_G}K\left(\boldsymbol{\chi}_{Ij},\widehat{\xi}_G\right)\,\widehat{\sigma}_G\left(\widehat{\xi}_G\right)\mathrm{d}L_G+\\
&\frac{1}{4\pi\gamma}\int\int_{\xi_I\in\Gamma_I}\left(\frac{1}{r(\boldsymbol{\chi}_{Ij},\xi_I)}+\frac{1}{r(\boldsymbol{\chi}_{Ij}^{'},\xi_I)}\right)\sigma_I(\xi_I)\,\mathrm{d}\Gamma_I+\\
&\frac{1}{4\pi}\int\int_{\xi_I\in\Gamma_I}\left[\left(\nabla\left(\frac{1}{r(\boldsymbol{\chi}_{Ij},\xi_I)}\right)+\nabla\left(\frac{1}{r(\boldsymbol{\chi}_{Ij}^{'},\xi_I)}\right)\right)\cdot\mathbf{n}(\xi_I)\right]\\
&V_I(\xi_I)\,\mathrm{d}\Gamma_I-\frac{1}{2}V_I(\boldsymbol{\chi}_{Ij})=0\,,\qquad j=1,\ldots,n_{cp_I}
\end{aligned}\tag{15}$$

where $n_{cp_I}$ is the number of collocation points in $\Gamma_I$. Kernel $K(\boldsymbol{\chi}_{Ij},\widehat{\xi}_G)$ is obtained after solving the integral in the circumferential perimeter $C_G$.

1. Equation from the compatibility condition applied on the interior problem:

$$\frac{1}{4\pi\gamma_I}\int\int_{\xi_I\in\Gamma_I}\frac{1}{r(\boldsymbol{\chi}_{Ij},\boldsymbol{\xi}_I)}\sigma_I(\boldsymbol{\xi}_I)\,d\Gamma_I+$$
$$\frac{1}{4\pi}\int\int_{\xi_I\in\Gamma_I}\left[\nabla\left(\frac{1}{r(\boldsymbol{\chi}_{Ij},\boldsymbol{\xi}_I)}\right)\cdot\mathbf{n}(\boldsymbol{\xi}_I)\right]V_I(\boldsymbol{\xi}_I)\,d\Gamma_I+ \quad (16)$$
$$\frac{1}{2}V_I(\boldsymbol{\chi}_{Ij})=0\,,\qquad j=1,\ldots,n_{cp_I}$$

The above integral equations are solved through the BEM. It should be noted that this numerical method is based on a discretization procedure which requires two types of approximation: the geometrical and the functional. The geometrical discretization consists of a subdivision of boundaries $\Gamma_G$ and $\Gamma_I$ into $n_{el_G}$ and $n_{el_I}$, respectively. On the other hand, the functions are approximated at each element by writing them in terms of their values at some fixed points in the element, called nodal points ($n_{np_G}$ in $\Gamma_G$, and $n_{np_I}$ in $\Gamma_I$), through interpolation functions.

As a result, the discretized equations can be expressed as a system of linear equations:

$$\begin{pmatrix}\mathbf{R}_{GG} & \mathbf{R}_{GI} & \mathbf{S}_{GI}\\ \mathbf{R}_{IG} & \mathbf{R}_{II} & \mathbf{S}_{II}\\ \mathbf{0} & \mathbf{T}_I & \mathbf{S}_I\end{pmatrix}\begin{pmatrix}\widehat{\boldsymbol{\sigma}}_G\\ \boldsymbol{\sigma}_I\\ \mathbf{V}_I\end{pmatrix}=\begin{pmatrix}\boldsymbol{\nu}_G\\ \mathbf{0}\\ \mathbf{0}\end{pmatrix} \quad (17)$$

where:

- $\mathbf{R}_{GG}$ is a square $(n_{cp_G}\times n_{cp_G})$ matrix, and $\mathbf{R}_{GI}$ and $\mathbf{S}_{GI}$ are $(n_{cp_G}\times n_{cp_I})$ matrices. Their terms come from integral Eq. (14).
- $\mathbf{R}_{IG}$ is a $(n_{cp_I}\times n_{cp_G})$ matrix, and $\mathbf{R}_{II}$ and $\mathbf{S}_{II}$ are square $(n_{cp_I}\times n_{cp_I})$ matrices. Their terms come from integral Eq. (15).
- $\mathbf{T}_I$ and $\mathbf{S}_I$ are square $(n_{cp_I}\times n_{cp_I})$ matrices, whose terms come from integral Eq. (16).
- $\boldsymbol{\sigma}_G$, $\boldsymbol{\sigma}_I$ and $\mathbf{V}_I$ are the unknown vectors.
- $\boldsymbol{\nu}_G$ is the vector which contains the boundary condition of the problem.
- The matrix is full and non-symmetric.

Once the unknowns $\sigma_G$, $\sigma_I$ and $V_I$ have been determined, the electric potential at any point in the ground and the main parameters of the grounding system can be calculated.

Before proceeding with the grounding system analysis, two of the most important steps in the numerical approach must be highlighted:

#### 2.3.1. Discretization procedure

The BEM is a method based on a discretization procedure, where the unknown functions are calculated on the boundary of the domains. To deal with this problem a linear parametric representation is defined: one-dimensional linear elements for approximating the axial line of the electrodes and two-dimensional linear elements for the enclosure surface.

The point collocation method is an appropriate method when the boundary surfaces of domains are smooth. However, when the geometry presents corners and/or edges, serious numerical problems appear with the collocation approach [17,18]. The problem is caused by the ambiguity in the normal vector along an edge or at a corner where a non-uniquely normal vector is defined. On the case of the enclosure, the geometry is similar to a parallelepiped and each planar side has a normal vector, but corners and edges present the mentioned issue.

Thus, an improved technique which involves moving the nodal and the collocation points from the edges and corners to the interior of the elements a certain distance $\lambda$ is chosen [19]. This technique is called semidiscontinuous method and optimal values for $\lambda$ can be found in the literature, as $0.75<\lambda<0.95$.

#### 2.3.2. Integration of kernels

The integration is important to obtain accurate and stable results. In this research, two types of integrals are differentiated, which have been solved through numerical techniques:

1. Regular integrals refer to all kernels where $\chi$ and $\xi$ do not belong to the same element. Therefore, the integrals are not singular and they are evaluated through the Gauss-Legendre quadrature.
2. Weakly singular integrals which refer to all kernels where the collocation point is located on the element analyzed or on an adjacent element to the analyzed one. The singularity of the kernel is of order $O(1/r)$.

   To calculate the integrals numerically over one-dimensional elements, a numerical approach based on the Element Subdivision Technique [20] and the Gauss-Legendre formula was developed. Similarly, for the integrals over two-dimensional elements, the numerical approach developed is based on the Lachat-Watson Transformation [21]. This technique consists in splitting up the integrated parent element into triangular subelements and defining a local coordinate system for each one. By this procedure, the Jacobian of the transformation is equal to zero in the point of singularity and it is cancelled out. Finally, the two-dimensional weakly integrals are calculated with accuracy through the Gauss-Legendre quadrature.

## 3. Industrial application: grounding system analysis

This section shows the principal objective of the developed formulation which is to calculate the main parameters of the protection system of real underground electrical substations. Thus, this formulation allows to design and analyze any grid configuration and to ensure that the grounding system does not exceed the safe voltage limits.

In order to show its application, two real examples will be analyzed (real images of the proposed examples can be found in [15]). The results obtained are the main parameters of grounding systems, which are the grid resistance, the GPR and the step and mesh voltage, as well as the surface and step voltage distributions.

### 3.1. Example I

In this first example, a grounding grid for a commercial underground electrical substation with dimensions 5.40 m × 2.46 m × 2.84 m will be analyzed. Each face of the enclosure is divided in a 10x10 grid which, by the authors experience, gives a enough accuracy in the results. Thus 600 elements with 726 degrees of freedom are used for the enclosure.

The general and numerical data used in the analysis are shown in Table 1, where the difference between the soil resistivity, 50 Ω m, and

**Table 1**
Example 1.

| GENERAL DATA | |
|---|---|
| Operating voltage | 20 kV |
| Grid current | 1000 A |
| Soil resistivity | 50 Ω m |
| Concrete resistivity | 3000 Ω m |
| NUMERICAL DATA | |
| Numerical approach | PCM |
| BEM elements | Linear ($\lambda$ = 0.85) |
| No. of elements (electrodes) | 14 |
| Degrees of freedom (electrodes) | 12 |
| No. of elements (enclosure) | 600 |
| Degrees of freedom (enclosure) | 726 |
| RESULTS | |
| Grid resistance (Ω) | 3.005 |
| GPR (V) | 3005.0 |
| Mesh voltage (V) | 937.897 |
| Step voltage (V) | 443.222 |

the concrete resistivity, 3000 Ω m [22], is highlighted. Another important datum is that a total grid current of 1000 A is supposed as the fault situation.

As depicted in Fig. 2, the grounding grid is formed by two perimeter rings connected between them, one located in the base of the excavation at 0.4 m from the enclosure, and another at a depth of 0.8 m under the ground surface and 1 m far from the enclosure. The bare copper conductors have a cross-sectional area of 50 $mm^2$. In this case, 14 elements are used to discretize the rods connected at 12 nodes.

After the analysis with the formulation proposed is carried out, the grid resistance, the GPR, the mesh voltage and the maximum step voltage are obtained (Table 1). The simulation time needed to perform the analysis was slightly greater than 20 min (1356 s) in a common personal computer (Intel Core i7-3820, 3.60 Ghz, RAM 24.0 GB). 95% of the time was invested in computing the surface and step voltage distributions, in this case with 600 elements and 726 integration points.

In addition to these main parameters, the surface and step voltage distributions have been calculated. A general 3D view of these potential distributions is presented in Fig. 3. The total area where the voltage distributions have been calculated is a rectangle of 14 m by 12 m, which implies a surface of 168 $m^2$ and in which 1600 points are analyzed.

More deeply, the surface and step voltage distributions over the area studied are depicted in Figs. 4 and 5. As shown in Fig. 4, the largest voltages during this fault situation appear just above the underground substation and the largest gradients arise at the perimeter areas. It should be noted that the largest voltages present a fairly uniform distribution. Owing to the largest gradients, the largest step voltages appear at the perimeter areas, and thus, it can be stated that the safest area (area with low step voltages values) is located above the underground substation (Fig. 5).

It must be mentioned that all distributions presented have a symmetrical solution, as it was expected since the grounding system is also symmetric.

A secondary result of the grounding system analysis with the developed formulation is to obtain the voltage and current density distributions over the enclosure (Figs. 6 and 7).

In Fig. 6, the voltage distribution over the enclosure surface is depicted. As can be seen, the highest voltage values are located on the areas closer to the grid and the voltages at the top are higher that at the bottom, which presents the lowest values. This is because the top is situated at 0.1 m from the ground surface, and therefore, the voltages are not dissipated. However, the space behind the bottom is infinite and the potentials can be dissipated into the ground.

Furthermore, Fig. 7 shows the current density distribution, where the negative values mean the current density entering the enclosure, and the positive ones, the current density that leaves it. In this case, the highest current densities appear on the underside of the enclosure, where their majority enter in the perimeter areas closer to the grid and leave it through the bottom.

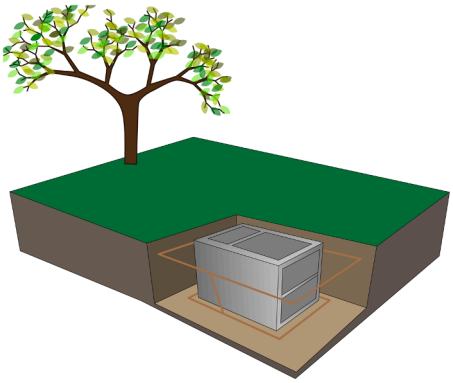

**Fig. 2.** Grounding system - Example I.

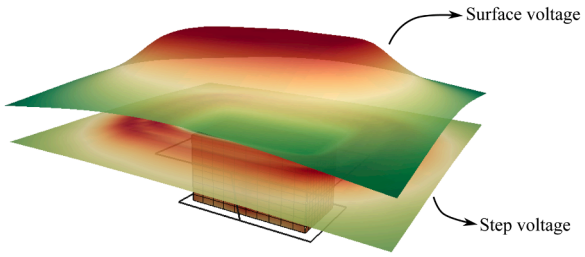


**Fig. 3.** 3D view of potential distributions - Example I.

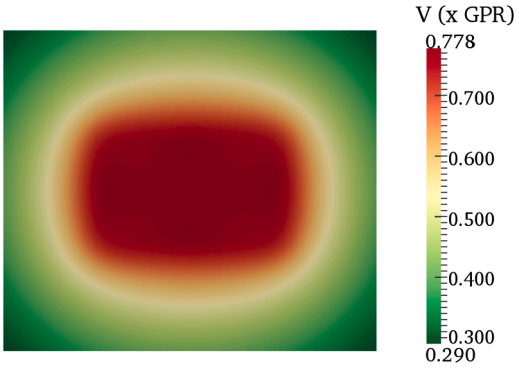


**Fig. 4.** Surface voltage distribution - Example I.

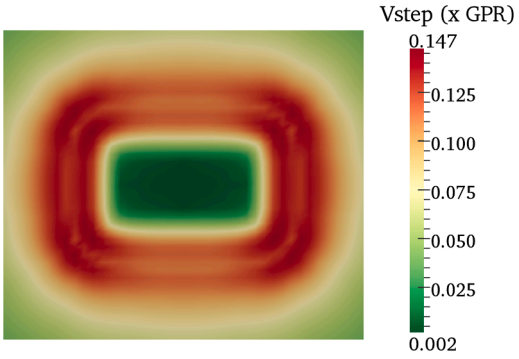


**Fig. 5.** Step voltage distribution - Example I.

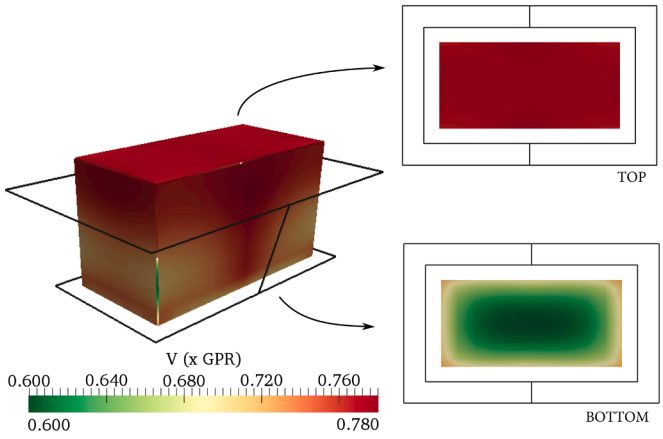


**Fig. 6.** Voltage distribution over the enclosure surface - Example I.

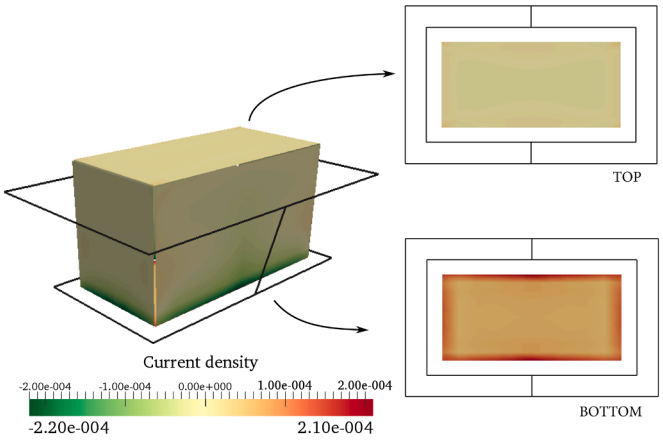


**Fig. 7.** Current density distribution over the enclosure surface - Example I.

A comparison of the example removing the underground substation, only with simulating the grounding system, was also carried out. Fig. 8 shows a comparison of the step voltage distribution on surface while Fig. 9 presents the net differences in both, surface and step voltage distributions over the area studied in voltage units.

As seen in Fig. 9, both the step voltage and the surface voltage distributions change between the two models. The step and surface voltage increase on the short sides of the grid and decrease over the long sides with the underground substation. In the model including the enclosure, the step voltage inside the grounding grid is lower even though the surface voltage increases.

### 3.2. Example II

In this second grounding system analysis, the grounding grid is formed by a rectangular 5 m × 3.5 m grid at a depth of 0.8 m under the ground surface and 1 m far from the enclosure and with eight 2-meter-long ground rods around its perimeter (Fig. 10). The conductor diameter is 8 mm, and for the ground rods the diameter is 14 mm. In this example, the rods are discretized. Rods on the long side of the substation are discretized in three elements while rods on the short side and ground rods are discretized in two elements. The model for the electrodes is thus formed by 36 elements and 36° of freedom. In this case, the enclosure dimensions are 3.46 m × 2.46 m × 2.35 m and the same 10x10 discretization is used as in the previous example.

The general data is defined in Table 2, where now the soil resistivity is 120 Ω m.

Again, after doing the analysis, the main parameters that characterize this grounding system are obtained (Table 2).

As in Example I, the surface and step voltage distributions have been calculated (Figs. 11 and 12). The total area studied is a rectangle of 12 m by 10 m, which implies a surface of 120 $m^2$ in which 1600 points are analyzed.

Fig. 11 shows that the largest surface voltages appear above the substation with a uniform distribution, and the largest step voltages arise at the perimeter area of the enclosure where the grid is located

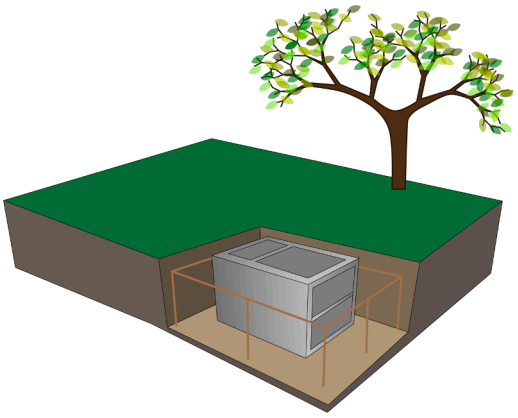

**Fig. 10.** Grounding system - Example II.

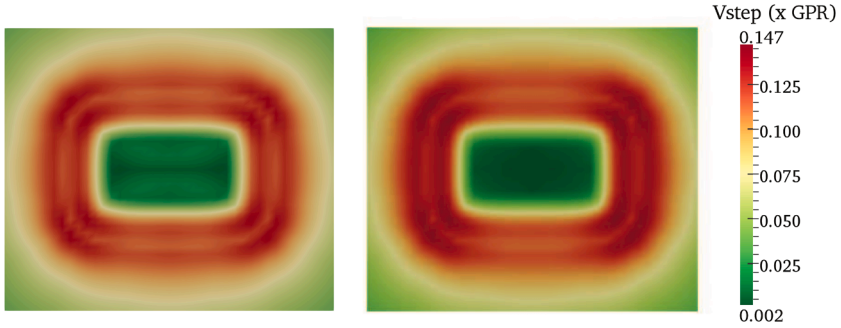


**Fig. 8.** Step voltage distribution over the enclosure surface without substation (left) and with substation (right) - Example I.

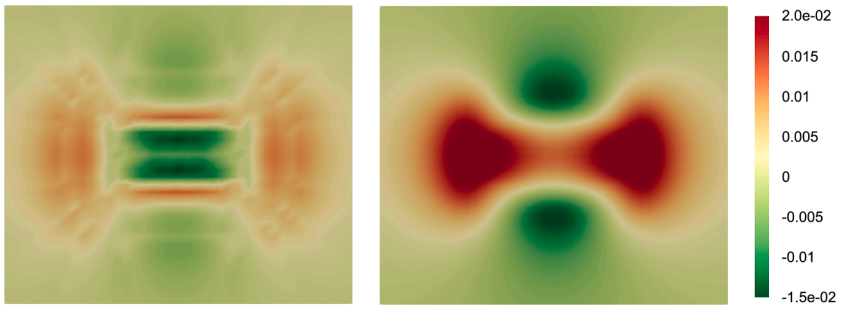


**Fig. 9.** Differences in step voltage (left) and surface voltage (right) between models with and without underground substation - Example I.

**Table 2**
Example 2.

| GENERAL DATA | |
|---|---|
| Operating voltage | 20 kV |
| Grid current | 1000 A |
| Soil resistivity | 120 Ω m |
| Concrete resistivity | 3000 Ω m |
| NUMERICAL DATA | |
| Numerical approach | PCM |
| BEM elements | Linear ($\lambda = 0.85$) |
| No. of elements (electrodes) | 36 |
| Degrees of freedom (electrodes) | 36 |
| No. of elements (enclosure) | 600 |
| Degrees of freedom (enclosure) | 726 |
| RESULTS | |
| Grid resistance (Ω) | 8.430 |
| GPR (V) | 8430 |
| Mesh voltage (V) | 2552.756 |
| Step voltage (V) | 1212.386 |

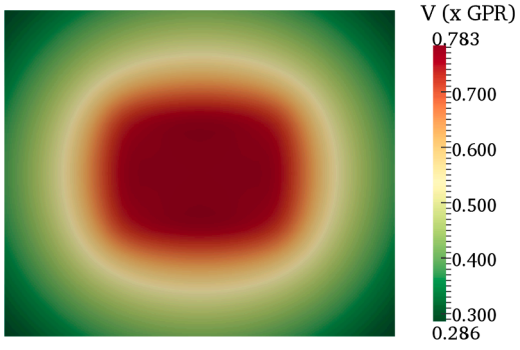


**Fig. 11.** Surface voltage distribution - Example II.

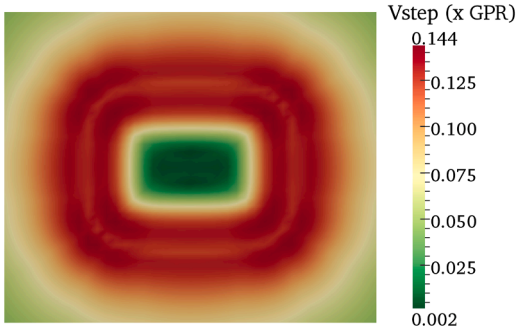


**Fig. 12.** Step voltage distribution - Example II.

(Fig. 12). Although the voltage values have changed regarding the analysis of Example I, the figures depict similar distributions.

As it has been done in Example I, the voltage and current density distributions over the enclosure are obtained (Figs. 13 and 14). Similarly, the highest voltage values are located on the areas closer to the grid and the voltages at the top are higher than at the bottom, which presents the lowers values. The highest current densities appear on the underside of the enclosure, where their majority enter in the perimeter areas closer to the grid and leave it through the bottom.

Additionally, the voltage profiles along a horizontal line that crosses the middle of the area analyzed are represented in Figs. 15 and 16. Fig. 15 depicts the surface voltage profile where the maximum surface voltage appears above the substation with constant value along all the length and the highest gradients are just located before this maximum, as explained above. Furthermore, Fig. 16 presents the step voltage

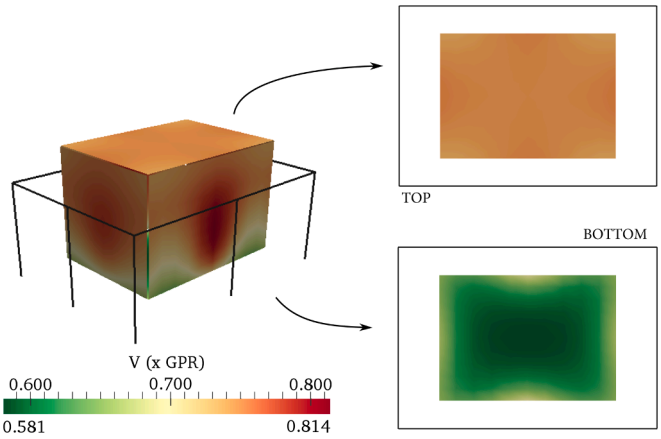


**Fig. 13.** Voltage distribution over the enclosure surface - Example II.

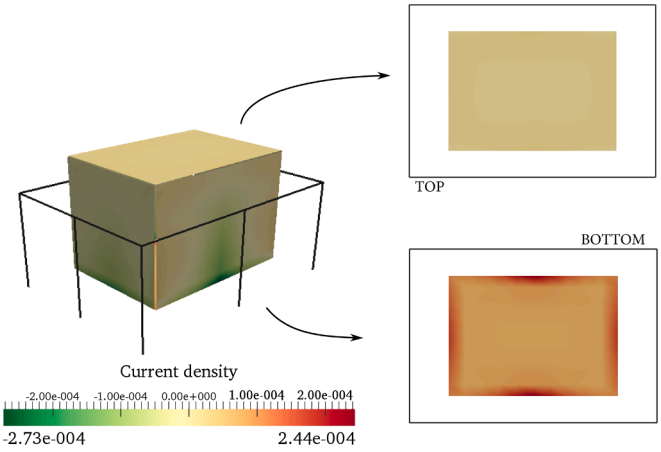


**Fig. 14.** Current density distribution over the enclosure surface - Example II.

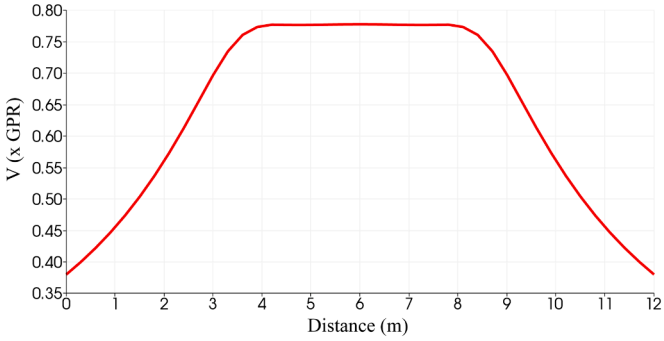


**Fig. 15.** Surface voltage profile - Example II.

profile in which due to the surface voltage gradients, two peaks arise in the step voltage profile coinciding with the perimeter grid location and a plain appears where the potential gradients are minima.

## 4. Conclusion

Grounding systems are essential devices to ensure and guarantee secure conditions in electrical substations for the facility and the safety of individuals. Their analysis has always been an important issue in electrical engineering, but it is with the emergence of underground electrical substations and their urban character, which is surrounded by residential buildings, green areas, parks or commercial areas, where a

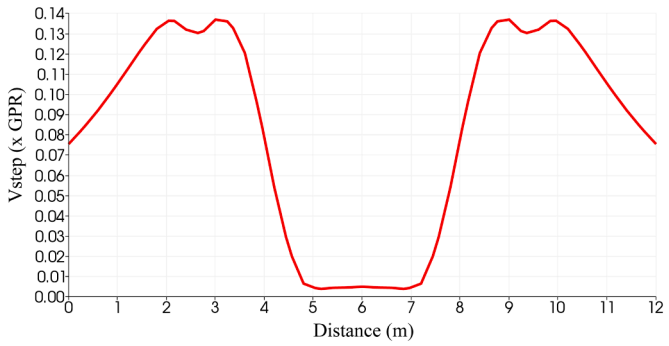


**Fig. 16.** Step voltage profile - Example II.

properly grounding system analysis is even more essential.

In this paper, a mathematical and numerical approach to design and analyze the grounding systems of underground electrical substation was presented. This formulation, based on the general equations of electromagnetism, allows to model a more realistic soil structure, where the underground electrical substation is embedded in the ground. Thus, more realistic results are obtained for their main parameters.

The proposed approach has been validated against benchmark examples from the IEEE. Two real examples have been presented in this paper. These examples showed that the main parameters of grounding grid can be calculated with the proposed formulation, as well as the surface and step voltage distributions. In addition, the voltage and current densities over the enclosure can also be calculated, and the formulation is adaptable to different and variable grounding systems and geometries. The approach developed and validated could be adapted to stratified or multilayer soils to increase its range of application.

## Dedication

In memory of Professor Manuel Casteleiro.

## Declaration of Competing Interest

The authors declare that they have no known competing financial interests or personal relationships that could have appeared to influence the work reported in this paper.

## Declaration of Competing Interest

None

## Acknowledgments

This work has been partially supported by the “Consellería de Cultura, Educación e Ordenación Universitaria” of the “Xunta de Galicia” (grant GRC2014/039) and (grant ED431C2018/41), by the “Ministerio de Economía y Competitividad” (grant DPI2015-68431R) and "Ministerio de Ciencia, Innovación y Universidades" (grant RTI2018-093366-B-I00). Funding for open access charge: Universidade da Coruña/CISUG

## References

[1] J. Nahman, D. Jelovac, Risk of fatal electric shocks at distribution network MV/LV transformer stations, IEE Proc.-Gener. Transm. Distrib. 145 (4) (1998) 463–467.
[2] J. Nahman, D. Jelovac, High-voltage/medium(low)-voltage substation earthing systems, IEE Proc. 134 (1) (1987) 75–80.
[3] G. SSM, K.A. Shoush, Analytical methods for earth surface potential calculation for grounding grids, Int. J. Eng. Comput.Sci. 13 (3) (2013) 47–53.
[4] Z.G. Datsios, P.N. Mikropoulos, Safety performance evaluation of typical grounding configurations of MV/LV distribution substations, Electr. Power Syst. Res. 150 (2017) 36–44.
[5] F. Freschi, F. Mitolo, M. Tartaglia, An effective semianalytical method for simulating grounding grids, IEEE Trans. Ind. Appl. 49 (1) (2013) 256–263.
[6] L. Zx, J.B. Fan, W.J. Chen, Numerical simulation of substation grounding grids buried in both horizontal and vertical multilayer earth model, Int. J. Numer. Methods Eng. 69 (11) (2007) 2359–2380.
[7] J. Liu, F.P. Dawalibi, Wind turbine farm network grounding design using integrated simulation methods and techniques. Proceedings of the International Conference on Future Power and Energy Engineering, 2010.Shenzhen, China
[8] F. Freschi, M. Mitolo, M. Tartaglia, Interferences phenomena between separate grounding systems, IEEE Trans. Ind. Appl. 50 (4) (2014) 2853–2860.
[9] S. Fortin, N. Mitskevitch, F.P. Dawalibi, Analysis of grounding systems in horizontal multilayer soils containing finite heterogeneities, IEEE Trans. Ind. Appl. 51 (6) (2015) 5095–5100.
[10] I. Colominas, F. Navarrina, M. Casteleiro, A boundary element numerical approach for grounding grid computation, Comput. Method Appl. Mech. Eng. 174 (1999) 73–90.
[11] I. Colominas, J. Gómez-Calviño, F. Navarrina, M. Casteleiro, Computer analysis of earthing systems in horizontally or vertically layered soils, Electr. Power Syst. Res. 59 (3) (2001) 149–156.
[12] I. Colominas, J. París, D. Fernández, F. Navarrina, M. Casteleiro, Numerical simulation tool for multilayer grounding analysis integrated in an open-source CAD interface, Int. J. Electr. Power Energy Syst. 45 (2013) 353–361.
[13] I. Colominas, J. París, R. Guizán, F. Navarrina, M. Casteleiro, Numerical modeling of grounding systems for aboveground and underground substations, IEEE Trans. Ind. Appl. 51 (6) (2015) 5107–5115.
[14] IEEE, Guide for safety in AC substation grounding, IEEE Standard 80 (2013).
[15] R. Guizán. A General Formulation for Computational Design of Grounding Systems in Underground Electrical Substations, Dept. Mat. Aplicada, UDC, A Coruña, Spain, 2018.
[16] O.C. Zienkiewicz, R.L. Taylor, J.Z. Zhu, The Finite Element Method: its Basis and Fundamentals, seventh ed., Elsevier, 2013.
[17] E.T. Ong, K.M. Lim, Three-dimensional singular boundary elements for corner and edge singularities in potential problems, Eng. Anal. Bound. Elem. 29 (2) (2005) 175–189.
[18] B.B. Guzina, R.Y. Pak, A.E. Martínez, Singular boundary elements for three-dimensional elasticity problems, Eng. Anal. Bound. Elem. 30 (8) (2006) 623–639.
[19] C. Patterson, M. Sheikh, Interelement Continuity in the Boundary Element Method, Topics in Boundary Element Research, Springer, US, 1984.
[20] M.H. Aliabadi, The Boundary Element Method. Volume 2: Applications in Solids and Structures, Wiley, 2002.
[21] J.C. Lachat, J.O. Watson, Effective numerical treatment of boundary integral equations: a formulation for three-dimensional elastostatics, Int. J. Numer. Methods Eng. 10 (1) (1976) 991–1005.
[22] S. Government, RD 337-2014, Reglamento sobre condiciones técnicas y garantías de seguridad en instalaciones eléctricas de alta tensión, ITC-RAT 01–23.